



1 **Increased Intensity and Frequency of Global Coastal Compound Wind and**

2 **Precipitation Extremes: Implications for Sea Level Anomalies**

3

4 Xinlong Zhang¹, Jiayi Fang², Yue Qin³, Weiping Wang^{4,*}, Ping Shen^{5,*}

5

6 ¹ State Key Laboratory of Internet of Things for Smart City and Department of Civil
7 and Environmental Engineering, University of Macau, Macao SAR, People's Republic
8 of China

9 ² Institute of Remote Sensing and Earth Sciences, Hangzhou Normal University,
10 Hangzhou, Zhejiang, People's Republic of China

11 ³ College of Environmental Sciences and Engineering, Peking University, Beijing,
12 People's Republic of China

13 ⁴ School of National Safety and Emergency Management, Beijing Normal University,
14 Zhuhai, Guangdong, People's Republic of China

15 ⁵ State Key Laboratory of Internet of Things for Smart City and Department of Ocean
16 Science and Technology, University of Macau, Macao SAR, People's Republic of
17 China

18

19

20

21 *Corresponding authors. Ping Shen: pingshen@um.edu.mo; Weiping Wang:

22 wpwang@bnu.edu.cn



23 **Abstract**

24 Coastal flooding and damage can result from compound extremes of wind and
25 precipitation that elevate sea level anomalies. However, the global patterns and impacts
26 of such conditions are poorly understood. Here we analyze observational and model
27 data to reveal a positive correlation between wind and precipitation extremes across
28 most of the global coastline, especially at higher latitudes. We also show that these
29 variables exhibit stronger dependence on higher quantiles, indicating more frequent and
30 severe compound conditions. Moreover, we demonstrate that sea level anomalies are
31 enhanced during compound conditions compared to normal conditions, implying
32 increased coastal flooding risk. We project that both the intensity and frequency of
33 compound conditions will rise in 2020-2100 compared to 1940-2014 under two
34 emission scenarios, with larger changes at high latitudes. Our findings highlight the
35 need for assessing and managing the risks and impacts of compound extremes on
36 coastal communities and infrastructure.

37

38 **Keywords:** Climate change; Extreme precipitation and wind; CMIP6; Sea level
39 anomalies



40 **1 Introduction**

41 Climate change and extreme weather conditions pose severe challenges for coastal
42 regions that are exposed to multiple hazards such as strong winds, storms, and flooding
43 (Hoegh-Guldberg et al., 2019; Mora et al., 2018). A particularly impactful class of
44 hazards are compound wind and precipitation extremes (CWPEs), which arise from the
45 joint occurrence of high wind speeds and heavy precipitation in some locations at the
46 same time (Bevacqua et al., 2021; Martius et al., 2016; Messmer and Simmonds, 2021;
47 Zscheischler et al., 2020). CWPEs can have devastating consequences for coastal
48 infrastructure, ecosystems, and human lives by exacerbating storm surges and waves,
49 resulting in elevated sea level anomalies (SLA) and coastal inundation (Davison et al.,
50 2023; Deb et al., 2023; Vousdoukas et al., 2022; Wahl et al., 2015).

51 CWPEs are often associated with large-scale atmospheric disturbances such as
52 extratropical cyclones (ETCs) and tropical cyclones (TCs) (Bermúdez et al., 2021; Gori
53 et al., 2022). ETCs are low-pressure systems that develop in the mid-latitudes and
54 generate strong winds and heavy rainfall along their fronts (Chen et al., 2010; Shaw et
55 al., 2016). TCs are intense low-pressure systems that originate over warm tropical
56 oceans and produce destructive winds, torrential rainfall, and storm surges that affect
57 the coastal areas they encounter. Both ETCs and TCs can induce CWPEs, which in turn
58 can elevate SLA and cause coastal flooding, damage, and disruption (Knutson et al.,
59 2010; Lionello et al., 2019; Maduwantha et al., 2024; Martín et al., 2023; Woodworth
60 et al., 2019). The occurrence of CWPEs is projected to increase under future climate
61 change (Yaddanapudi et al., 2022), potentially worsening the impacts of SLA on coastal
62 regions. To evaluate and manage the risks posed by these conditions in a warming world,
63 we need to understand and the consequences of CWPEs on SLA as well as their future
64 projections.

65 CWPEs have a high potential impact on SLA in coastal regions, yet their
66 occurrence, characteristics, and changes under different climate scenarios remain
67 poorly understood. Previous studies have largely examined single-variable extremes,
68 such as precipitation (Bevacqua et al., 2020; Jiang et al., 2020) or wind speed (Wu et
69 al., 2020; Zha et al., 2020), or have been restricted to specific regions or seasons
70 (Maduwantha et al., 2024; Moustakis et al., 2021; Yaddanapudi et al., 2022). Few
71 studies have investigated CWPEs in global coastal areas. Furthermore, the impact of
72 global coastal CWPEs conditions on SLA, especially under future climate change, has
73 not been well evaluated, despite its importance. Hence, a comprehensive and systematic



74 assessment of CWPEs and their impact on SLA in global coastal regions is warranted.

75 In this study, we aim to fill this knowledge gap by addressing the following
76 research questions: (1) How do CWPEs vary across global coastal regions in terms of
77 frequency and spatial extent? (2) How do CWPEs conditions change under different
78 climate scenarios compared to the historical period? (3) What is the impact of CWPEs
79 on SLA in global coastal regions under historical and different climatic scenarios? To
80 answer these questions, we use a combination of observational data from various
81 sources and model data from the Coupled Model Intercomparison Project Phase 6
82 (CMIP6). We first defined the CWPEs and then we used the copula model to calculate
83 the joint probabilities of these conditions and compare them with their independent
84 probabilities. We also calculate the mean value of SLA at the time of the composite
85 condition. Finally, we have used the CMIP6 model to make projections for different
86 future scenarios.

87

88 **2 Materials and methodology**

89 **2.1 Data**

90 We used gridded monthly observations and modelled data from various sources to
91 investigate the coupling between compound extreme wind speed and precipitation
92 conditions and their relationship to SLA. We obtained the meteorological data (10-m
93 wind speed and total precipitation) from the ERA5 reanalysis dataset, which covers the
94 global atmosphere and surface at an hourly temporal resolution and a $0.25^\circ \times 0.25^\circ$
95 spatial resolution. We utilized the monthly mean data extracted from this dataset due to
96 its ability to capture detailed meteorological variations with high precision. The ERA5
97 dataset is preferred for its extensive validation and proven reliability in numerous
98 climate studies, making it a trustworthy source for our analysis (Hersbach et al., 2020).
99 We acquired the SLA data from satellite observations provided by the Copernicus
100 Climate Change Service (C3S), which covers the global ocean at a daily temporal
101 resolution and a $0.25^\circ \times 0.25^\circ$ spatial resolution. We computed the monthly mean SLA
102 for each grid point from this data. Both datasets span the period 1993–2020. By
103 selecting these two datasets, we ensured a comprehensive and reliable analysis based
104 on their high resolution, global coverage, and consistency. The use of these specific
105 datasets allows for a detailed examination of the relationships between meteorological
106 conditions and sea level changes, furthering our understanding of global climate



107 patterns and their potential impacts.

108 We used 11 models from CMIP6 that provide monthly output of 10-m wind speed
109 ('sfcWind'), total precipitation ('pr'), and SLA ('zos') for the historical (1940–2014)
110 and future (2020–2100) periods under two scenarios: SSP245 (medium-low emissions)
111 and SSP585 (high emissions). See Supplementary Table S1 for model details. We
112 bilinearly interpolated all model data to a common $1^\circ \times 1^\circ$ grid. We removed the
113 seasonal effects from the SLA data by subtracting the monthly mean values for each
114 grid cell over the entire study period (both observed and CMIP6 data), effectively
115 isolating the seasonal cycle to focus on the interannual and long-term trends.

116 We obtained coastline data at a scale of 1:110m from Natural Earth
117 (<https://www.naturalearthdata.com/>). This dataset provides a comprehensive and
118 detailed representation of global coastlines, suitable for our study. Additionally, we
119 excluded small islands to focus on major coastlines, as small islands may not be well-
120 represented in our meteorological and sea level datasets due to their limited data
121 availability. We used this data to select meteorological grid points along the coastline.
122 We chose the grid point closest to the shoreline for each meteorological data grid cell
123 ($1^\circ \times 1^\circ$ grid) that intersected the shoreline. This approach ensures that we reflect the
124 meteorological conditions along the coastline as accurately as possible within the
125 constraints of the gridded dataset. Our analysis is limited to the range from 60°N to
126 60°S latitude primarily due to the quality and integrity of satellite observations used in
127 this study. At higher latitudes, data integrity and quality tend to be lower due to factors
128 such as increased cloud cover, atmospheric and instrument noise, and reduced solar
129 illumination (Gabarró et al., 2023). This can significantly impact the accuracy of sea
130 level anomaly (SLA) measurements, which are crucial for our analysis. Moreover, the
131 focus of this study is on global coastal regions, where most major coastal cities and
132 populations are concentrated within the 60°N to 60°S latitude band. Limiting our
133 analysis to this range allows us to focus on areas that are most vulnerable to the impacts
134 of compound extreme wind and precipitation conditions. As the CMIP6 data are
135 available in several models and with different resolutions between the models, to
136 harmonize the calculations and analyses, we use information from the nearest grid point
137 to the coastline to represent the meteorological and sea level conditions along the
138 coastline. We chose the grid cell for each meteorological data intersecting the coastline
139 as the grid point closest to the coastline. This approach ensures that we reflect the
140 meteorological conditions along the coastline as accurately as possible within the
141 constraints of the gridded dataset.



142

143 2.2 Statistical analysis

144 2.2.1 Combined precipitation and wind probability

145 Our research focuses on identifying long-term trends and spatial patterns in the
146 co-occurrence of these extreme conditions in coastal areas around the globe. By using
147 monthly rather than daily data, we are able to analyze broad trends across multiple years,
148 providing valuable insights into the potential impacts of climate change on coastal flood
149 risk. To identify extreme conditions, we used the 90th percentile of the historical
150 distribution as a threshold for both precipitation and wind in each grid cell (Meucci et
151 al., 2020). That is, CWPEs conditions are considered to have occurred when both
152 precipitation and wind speeds exceed the thresholds in a month at a grid point. To model
153 the dependence structure of precipitation and wind, we employed bivariate copulas,
154 which are flexible tools to capture the relationship between dependent variables .
155 Copulas can overcome the limitation of using a small sample size to estimate the co-
156 occurrence of extreme precipitation and wind, especially in regions where precipitation
157 and wind are weakly or negatively correlated (Zscheischler and Seneviratne, 2017). The
158 joint probability distribution of precipitation and wind can be expressed as

$$F_{X,Y}(x, y) = P(X \leq x, Y \leq y) \quad (1)$$

159 The marginal cumulative distribution of rainfall and wind is $F_X(x)$ and $F_Y(y)$.
160 $F_X(x) = P(X \leq x)$, $F_Y(y) = P(Y \leq y)$. Their joint distribution is then found by the
161 copulas model. Assuming that the cumulative distribution function of this joint
162 distribution is $C(u, v)$, the joint probability distribution of X and Y can be written as

$$F_{X,Y}(x, y) = C(F_X(x), F_Y(y)) \quad (2)$$

163 where $u = F_X(x)$, $v = F_Y(y)$, are the probability values of precipitation and wind
164 between 0 and 1.

165 Having obtained the joint distribution, the probability that they are both greater
166 than or equal to the 90th percentile can be calculated by the following formula.

$$\begin{aligned} &P(u > 0.9 \cap v > 0.9) \\ &= 1 + C(F_X(0.9), F_Y(0.9)) - C(F_X(0.9), F_Y(1)) \\ &\quad - C(F_X(1), F_Y(0.9)) \end{aligned} \quad (3)$$

167 So, the probability of this compound extreme condition is given by

$$\begin{aligned} P(u > 0.9 \cap v > 0.9) &= 1 + C(0.9, 0.9) - C(0.9, 1) - C(1, 0.9) \\ &= 1 + C(0.9, 0.9) - u - v \end{aligned} \quad (4)$$



168 where $F_X(0.9)$ and $F_Y(0.9)$ are the 90% quantile of precipitation and wind, respectively.

169 To estimate the co-occurrence probabilities of extreme conditions, we used
170 copulas to model the dependence of precipitation and wind. We fitted the data with five
171 prevalent bivariate copulas: Gaussian, Student-t, Clayton, Frank, and Gumbel. Each
172 copula is adept at capturing distinct forms of variable interdependence. To elaborate:
173 The Gaussian copula presupposes a multivariate normal distribution of variables,
174 making it apt for modeling symmetric dependencies, albeit with a potential
175 underestimation of tail dependence. The student-t copula, while similar to the Gaussian,
176 features heavier tails, thereby accommodating stronger tail dependence. The Clayton
177 copula excels at capturing lower tail dependence, proving beneficial in scenarios where
178 variables simultaneously tend towards extreme values in the same direction.
179 Contrastingly, the Frank copula exhibits no tail dependence but effectively models
180 positive dependence across the entire distribution range. Lastly, the Gumbel copula
181 specializes in upper tail dependence, suitable for when extremes in one variable align
182 with those of another. To ascertain the optimal copula fit for each grid cell, we compared
183 the log-likelihood magnitudes. This metric serves as a gauge for how accurately a
184 statistical model aligns with observed data, where higher values reflect a more precise
185 fit. Selecting the most fitting copula is pivotal, as it dictates the joint probability
186 distribution of precipitation and wind within each grid cell, forming the bedrock of our
187 analytical approach. By evaluating multiple copula varieties, we strive to ensure the
188 precision of our modeling reflecting the observed dependence patterns between
189 precipitation and wind extremes. We used empirical distributions of precipitation and
190 wind speed as the marginal distributions for our copula models. This choice allows us
191 to capture the full range of variability, including the extreme tails, in our analysis of
192 compound extreme conditions.

193 We used the probability multiplication factor (PMF) to quantify the joint
194 probability of a compound condition, which is the ratio of the joint probability of two
195 variables (accounting for their correlation) to the probability under the assumption of
196 independence (Ridder et al., 2020; Yaddanapudi et al., 2022). High values of PMF
197 (greater than 1) suggest a stronger dependence between extreme precipitation and wind
198 conditions, indicating that they tend to co-occur more frequently than expected under
199 independence. Conversely, low values of PMF (less than 1) imply a weaker dependence
200 between these variables, suggesting less frequent co-occurrence. We obtained the joint
201 probabilities under independence from the independent copula as follows: $P = 1 +$



202 $C(0.9,0.9) - u - v = 1 + 0.81 - 0.9 - 0.9 = 0.01$. The PMF can be expressed as

$$PMF = \frac{P(u > 0.9 \cap v > 0.9)}{0.01} \quad (5)$$

203 In calculating PMF for future scenarios, we have used the same approach as for
204 the historical period, maintaining the historical independence probability (0.01) in the
205 denominator. This allows us to isolate the changes specifically due to the joint
206 occurrence of extreme precipitation and wind conditions across historical and future
207 periods. We acknowledge that changes in the marginal distributions of precipitation and
208 wind may further impact the future compound effect. However, our primary focus in
209 this study is on assessing the relative change in the joint probability of extreme
210 conditions, taking into account the historical dependence structure as a reference.

211

212 **2.2.2 Compound extreme conditions and their impacts**

213 To quantify the coupling between precipitation and wind along the coastlines, we
214 examined their joint probability distribution and computed the Pearson's correlation
215 coefficient for each grid point over the global coastal area. We assigned coastal
216 precipitation and wind values to 10×10 percentile bins and calculated the mean
217 probability of each bin for each grid point. We also computed the mean SLA for each
218 bin by averaging the SLA values that corresponded to the precipitation and wind values
219 in that bin. This allowed us to assess the sea level response to different combinations of
220 precipitation and wind, especially to extreme conditions.

221 We analyzed the CMIP6 simulations of historical (1940–2014) and future (2020–
222 2100) scenarios under different emission pathways (SSP245 and SSP585) and
223 estimated the mean SLA associated with compound precipitation and wind extremes.
224 To isolate the changes in the joint occurrence of extreme events due to modifications in
225 the copula structure, we adopted a revised approach. Instead of utilizing future
226 thresholds, we focused solely on the changes in the joint distribution by using only the
227 90th percentile thresholds derived from the historical data, both for the historical period
228 and the future projections. This allows us to evaluate the frequency changes of
229 compound extreme events without confounding them with alterations in the marginal
230 distributions of precipitation and wind. Our analysis using historical thresholds serves
231 as a benchmark to assess changes in the frequency of extreme events similar to those
232 currently considered extreme. This approach clarifies how the occurrence of these
233 events is projected to evolve in the future. By maintaining a consistent threshold across



234 historical and future scenarios, we are able to more accurately attribute changes in the
235 probability multiplication factor (PMF) to modifications in the copula structure,
236 reinforcing our conclusions regarding the changes in compound extreme events under
237 future climate scenarios. In addition, we compared the 90th percentile of historical and
238 future precipitation and wind speeds to assess changes in the intensity of events that
239 calculate extremes.

240

241 **3 Results**

242 **3.1 Observed precipitation-wind coupling and compound extremes**

243 We used observational data to analyze the relationship between precipitation, wind,
244 and SLA on a global scale. We defined extreme conditions as those exceeding the 90th
245 percentile of the historical distribution for Precipitation and wind. We calculated the
246 Pearson's correlation coefficient between precipitation and wind for each grid cell. Fig.
247 S1a shows the global map of the correlation coefficients for the historical period (1993–
248 2020). The results indicate a positive correlation between precipitation and wind on a
249 global scale, with a mean value of 0.12 and a standard deviation of 0.38 (Fig. 1a and c).
250 The strength of the correlation varies from region to region, ranging from 0.89 in the
251 North Atlantic to -0.85 in northern South America. The correlation is generally stronger
252 at higher latitudes than at lower latitudes.

253 We computed the joint probability of extreme precipitation and wind conditions
254 for each grid cell using the copula approach, and in turn calculated the PMF. Fig. 1d
255 shows the PMF of extreme precipitation and wind conditions for the historical period.
256 The results reveal that extreme high values of precipitation and wind tend to co-occur
257 more frequently than expected by chance (Fig 1a and d). The PMF has a mean value of
258 1.91 and a standard deviation of 1.48. These results indicate a stronger dependence
259 between higher precipitation and wind values and emphasize that extreme conditions
260 are not independent and are largely co-occurring.

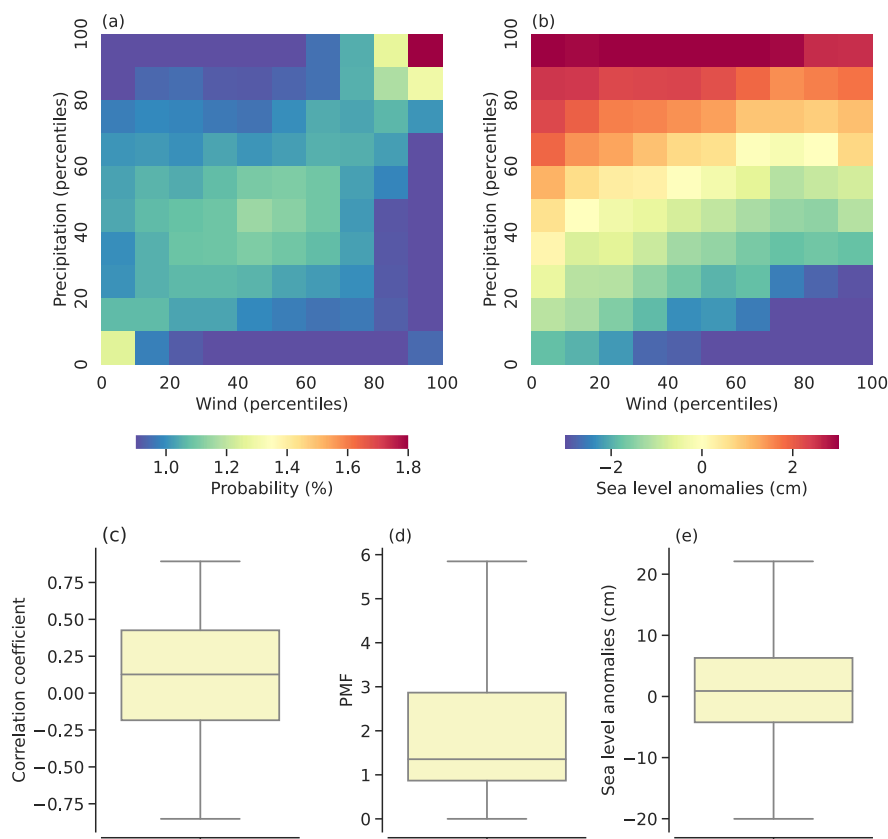
261 We calculated the Pearson's correlation coefficient between precipitation and SLA
262 (Fig. S1b), and between wind and SLA (Fig. S1c), for each grid cell over the coastal
263 areas. The results show that precipitation and SLA are positively correlated in most
264 regions, with a mean value of 0.21 and a standard deviation of 0.23, indicating that
265 higher precipitation is associated with higher SLA. The correlation between wind and
266 SLA is more complex, showing a non-linear and non-monotonic response. The mean



267 value is -0.04 and the standard deviation is 0.3.

268 We also calculated the mean value of the SLA at the time of the CWPEs for each
269 grid cell. Fig. 1e shows the mean SLA during CWPEs over the historical period. The
270 results show that under CWPEs, SLA are increased relative to normal conditions (Fig.
271 1b). The mean increase is 1.15 cm, and the standard deviation is 10.50 cm. The large
272 standard deviation reflects the large spatial heterogeneity. Therefore, it is important to
273 further identify spatial patterns and hotspot areas for compound extreme events in
274 current and future climate.

275



276

277 *Fig. 1 Coupling of precipitation and wind and their effect on coastal sea level*
278 *anomalies on the observed data (1993-2020).*

279 *(a) Average probability of each percentile bin for precipitation and wind. (b) Mean*
280 *values of SLA per percentile bin for precipitation and wind. (c) Pearson's correlation*
281 *coefficients for precipitation and wind. Values of PMF (d) and SLA (e) at compound*
282 *precipitation and wind extremes.*



283

284 **3.2 Increased intensity and frequency of compound extreme conditions in the**
285 **future**

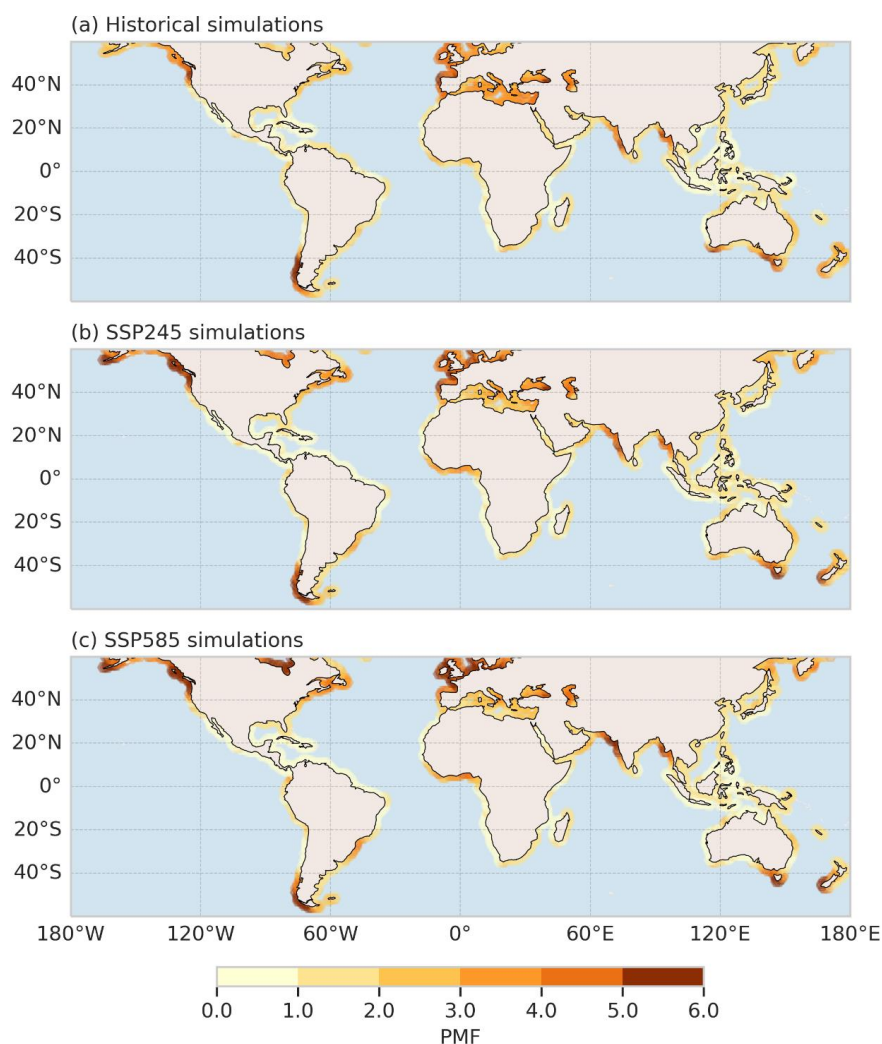
286 We examined the relationship between CWPEs under historical and different
287 future scenarios using 11 models from the CMIP6. The models simulated the historical
288 period (1940-2014) and the projected future period (2020-2100). All models showed a
289 positive correlation between precipitation and wind, as well as the bimodal distribution
290 observed in Fig. 1a (Fig. S2, S3 and S4), for the historical simulations. These model
291 results were consistent with observations from the ERA5 reanalysis data (Fig. 1a versus
292 Fig. S2, and Fig. S3 versus Fig. S4), suggesting that CMIP6 captures the extremes of
293 composite precipitation and wind realistically.

294 We applied copulas to model the bivariate distribution of precipitation and wind
295 in the CMIP6 simulations and to estimate PMF. Fig. 2a displays the spatial distribution
296 of PMF averaged across all models for the historical period. PMF is higher at higher
297 latitudes, especially in the coastal regions of northern Europe and Alaska. These areas
298 are prone to intense storms that may result from interactions between warm and cold
299 air masses that can enhance precipitation and wind speeds (Waliser and Guan, 2017;
300 Walsh et al., 2020). Moreover, the topography of these coastal areas, with their irregular
301 coastlines and steep mountains, can also affect the formation of extreme weather
302 conditions by altering the behavior of air masses and creating favorable conditions for
303 storm development. These regions also coincide with areas with high correlation
304 coefficients between precipitation and wind (Fig. S1a). PMF values are generally lower
305 in tropical and subtropical regions, where the positive correlation between precipitation
306 and wind is weaker.

307 PMF is projected to increase overall in future under both emission scenarios
308 compared to the historical period (Fig. 2b and c). The highest increases occur at high
309 latitudes, such as in coastal areas of northern Europe, Alaska, and Canada, where both
310 precipitation and wind intensity and frequency are expected to increase. Global mean
311 PMF values rose from 1.88 in the historical period to 1.98 in SSP 245 and 2.04 in SSP
312 585, implying a higher probability of future compound extreme conditions. In addition,
313 while the future thresholds for extreme wind speeds used to define compound extreme
314 conditions are almost constant (Fig. S5c and d), the thresholds for extreme precipitation
315 are higher (Fig. S5a and b), indicating that composite extreme conditions become more



316 extreme and more intense in the future.



317

318 *Fig. 2 PMF in CMIP6 models.*

319 *Model-averaged PMFs for extreme (above-90th percentile) precipitation and wind for*
320 *both historical simulations (1940-2014) and future simulations (2020-2100): (a) for*
321 *historical simulations, (b) for SSP245 future scenario, and (c) for SSP585 future*
322 *scenario. The thresholds used to define future extreme conditions are based on*
323 *historical.*

324

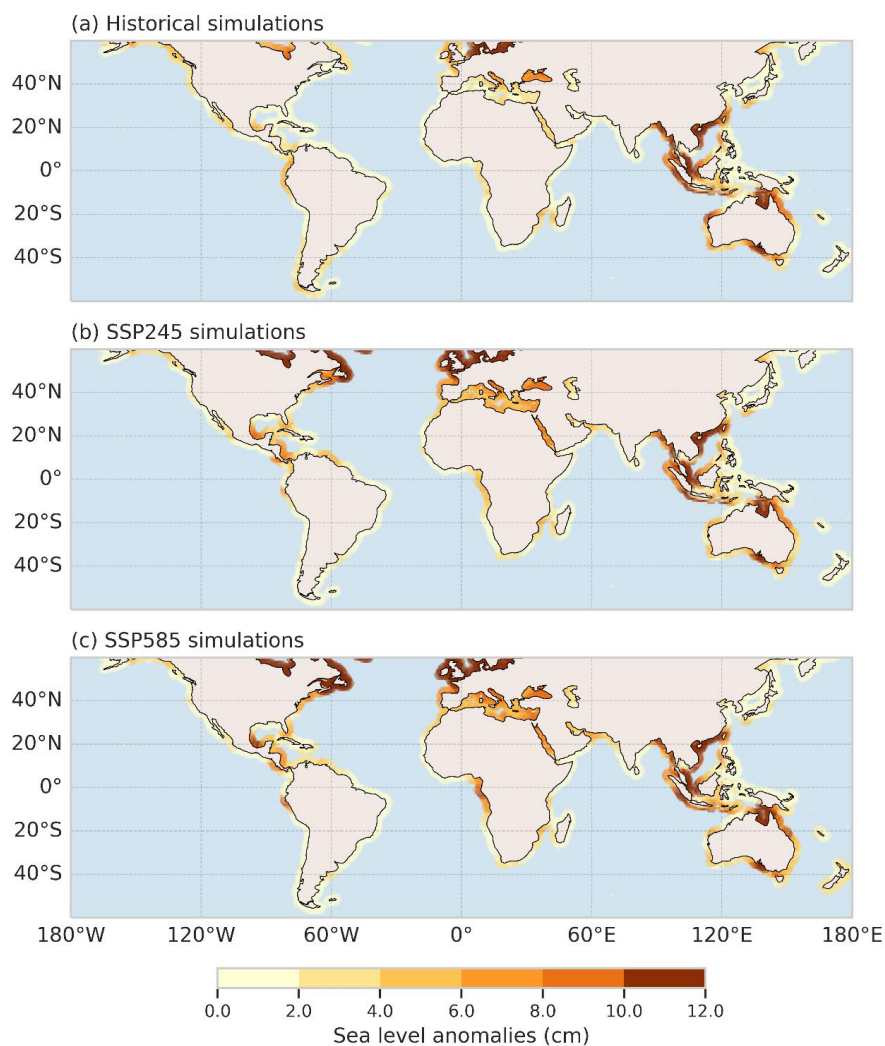


325 **3.3 SLA due to compound extreme conditions**

326 We estimated the mean SLA for each grid cell in the coastal zone when extreme
327 precipitation and wind conditions coincided to evaluate the impact of compound
328 extreme conditions on SLA. Fig. 3a presents a global map of the average SLA over the
329 historical period. The results indicate that SLA during compound extreme conditions is
330 positive in almost all regions, with a global mean of 2.7 cm. SLA is highest at high
331 northern hemisphere latitudes, exceeding 15 cm in some regions, and decreasing
332 slightly in most other regions between 60°S and 50°N (Fig. 3a and Fig. 4a). In both
333 future scenarios, SLA increases more at higher emissions (Fig. 3b and c). Based on
334 historical thresholds, in the future, compound extreme conditions lead to higher SLA
335 with a global mean of 4.5 cm for SSP245 and 5.0 cm for SSP585. These results suggest
336 that the impact of compound extreme conditions on SLA will increase in the future.

337 We also estimated the mean value of the SLA at the time of extreme precipitation
338 conditions and extreme wind conditions separately for each grid cell over coastal areas
339 using univariate thresholds. Fig. 5 presents the global maps of the mean SLA for
340 precipitation and wind extremes. In historical simulations, extreme precipitation has a
341 high impact on SLA in coastal areas such as northern Europe and northern Australia,
342 and extreme winds have a high impact on SLA in coastal areas such as northern Europe
343 and southern China (Fig. 5a and d). In future simulations, the impact of extreme
344 precipitation on SLA increases in almost all regions (Fig. 5a, b and c), while the impact
345 of extreme winds on SLA increases significantly at high northern hemisphere latitudes
346 and remains almost unchanged elsewhere (Fig. 5d, e and f). The results indicate that in
347 both historical and future simulations, the impact of precipitation on SLA is stronger
348 than that of wind in most regions, with global mean values of 2.7 cm and 0.08 cm in
349 the historical period respectively (Fig. 6). Only at high northern hemisphere latitudes is
350 the impact of wind strong (Fig. 6). This also coincides with a stronger positive
351 correlation between precipitation and SLA than between wind and SLA. The
352 importance of analyzing compound extreme conditions is also highlighted by the fact
353 that the area of high impact of compound conditions on SLA differs from that of
354 individual variables (Fig. 5 versus Fig. 3).

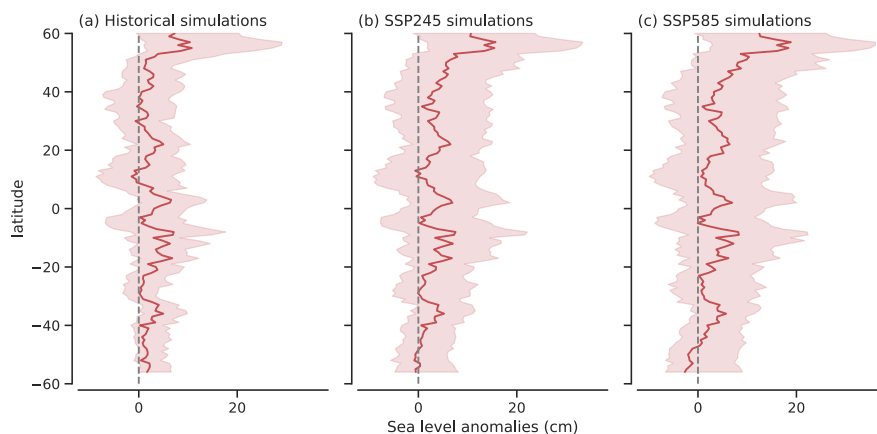
355



356

357 *Fig. 3 SLA due to compound extreme conditions in CMIP6 models.*

358 *Model-averaged SLA for extreme (above-90th percentile) precipitation and wind for*
359 *both historical simulations (1940-2014) and future simulations (2020-2100): (a) for*
360 *historical simulations, (b) for SSP245 future scenario, and (c) for SSP585 future*
361 *scenario. The thresholds used to define future extreme conditions are based on*
362 *historical.*

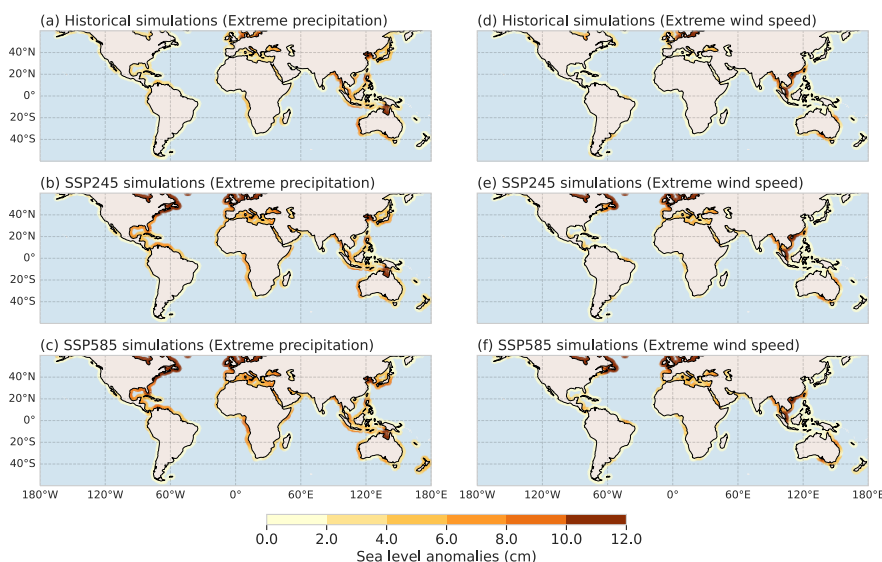


363

364 *Fig. 4 Distribution of SLA along latitude due to compound extreme conditions in the*
365 *CMIP6 model.*

366 *Distribution of SLA along latitude due to extreme (above-90th percentile) precipitation*
367 *and wind for both historical simulations (1940-2014) and future simulations (2020-*
368 *2100): (a) for historical simulations, (b) for SSP245 future scenario, and (c) for SSP585*
369 *future scenario. The solid lines are the multi-model mean of the SLA and the shading*
370 *indicates the 11 GCM 5th and 95th percentiles in CMIP6. The thresholds used to define*
371 *future extreme conditions are based on historical.*

372



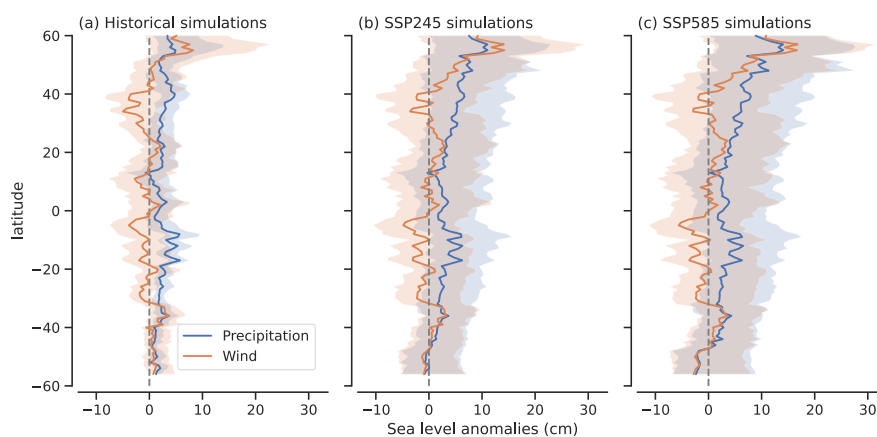
373

374 *Fig. 5 Impact of extreme precipitation and wind on SLA in the CMIP6 model.*

375 *SLA due to extreme (above-90th percentile) precipitation or wind in historical*



376 simulations (1940–2014) (a and d), in future SSP245 simulations (2020–2100) (b and
377 e), and in future SSP585 simulations (c and f). The thresholds used to define future
378 extreme conditions are based on historical.
379



380

381 *Fig. 6 Distribution of SLA along latitude due to extreme precipitation or wind*
382 *conditions in the CMIP6 model.*

383 *Distribution of SLA along latitude due to extreme (above-90th percentile) precipitation*
384 *or wind for both historical simulations (1940-2014) and future simulations (2020-2100):*
385 *(a) for historical simulations, (b) for SSP245 future scenario, and (c) for SSP585 future*
386 *scenario. The solid lines are the multi-model mean of the SLA and the shading indicates*
387 *the 11 GCM 5th and 95th percentiles in CMIP6. The thresholds used to define future*
388 *extreme conditions are based on historical.*
389

390 **4 Discussion and conclusions**

391 In this study, we examined how compound extreme conditions of precipitation and
392 wind affect SLA along global coastlines. We combined observational data and model
393 simulations to assess the historical and future changes of these conditions under
394 different emission scenarios. We found that:

- 395 (1) Precipitation and wind are globally and positively correlated, with a stronger
396 coupling at higher latitudes.
- 397 (2) Extreme high values of precipitation and wind co-occur more often than
398 expected by chance, indicating a higher dependence between these variables
399 at the upper tail of their distributions.
- 400 (3) Compound extreme conditions of precipitation and wind are linked to higher



401 SLA than normal conditions, implying an influence of these conditions on
402 coastal flooding risk.

403 (4) The intensity and frequency of compound extreme conditions are projected to
404 increase in the future under both emission scenarios, with a larger increase at
405 high latitudes, resulting in higher SLA during these conditions.

406 These findings address our research questions and confirm our hypotheses that
407 compound extreme conditions of precipitation and wind have a significant impact on
408 SLA and that this impact will amplify in the future due to climate change.

409 We explored the relationship between precipitation, wind, and SLA on a global
410 scale, which has been largely overlooked in previous studies. Most of the existing
411 studies have focused on regional or local scales, or on single variables such as
412 precipitation or wind (Bui et al., 2023; Chen et al., 2017; Zittis et al., 2022). We are
413 among the first to assess the global distribution and co-occurrence of extreme
414 precipitation and wind conditions and their influence on SLA using a copula approach.

415 We found that precipitation and wind are globally and positively correlated, with
416 a stronger coupling at higher latitudes. This coupling can be attributed to several
417 physical mechanisms, such as the development of low-pressure systems that produce
418 strong winds and heavy rainfall, the intensification of moisture transport by winds that
419 increases precipitation intensity, or the feedback between surface fluxes of heat and
420 moisture that affect both precipitation and wind (Back and Bretherton, 2005; Martius
421 et al., 2016). The coupling strength varies across regions, depending on factors such as
422 topography, land-sea contrast, orography, or ocean currents (Chen and Zhang, 2009;
423 Zscheischler et al., 2021). We also found that the probability of extreme high values of
424 precipitation and wind occurring together was higher than the probability of both
425 occurring independently, indicating a higher dependence between these variables at the
426 upper tail of their distributions. This dependence is measured by the PMF, which is the
427 ratio of the joint probability of compound extreme conditions to the probability under
428 independence. We found that PMF is higher at higher latitudes, especially in coastal
429 regions that are exposed to intense storms. These regions also correspond to areas with
430 high correlation coefficients between precipitation and wind. These results imply that
431 compound extreme conditions are not independent and are largely co-occurring.

432 We also showed that compound extreme conditions of precipitation and wind are
433 linked to higher SLA than normal conditions, implying an influence of these conditions
434 on coastal flooding risk. SLA are affected by several factors, such as atmospheric
435 pressure, wind stress, wind direction, ocean currents, waves, tides, or storm surges



436 (Woodworth et al., 2019; Zubier and Eyouni, 2020). Precipitation and wind can
437 influence SLA directly or indirectly through these factors. For instance, precipitation
438 can increase river runoff and coastal freshwater discharge, which can elevate sea level
439 locally (Dykstra and Dzwonkowski, 2021; Muis et al., 2016). Wind can generate storm
440 surges by pushing water towards the shore or by altering ocean currents and waves. We
441 found that in most regions, precipitation has a stronger influence on SLA than wind,
442 except at high northern hemisphere latitudes where wind has a strong influence. This
443 also corresponds to a stronger positive correlation between precipitation and SLA than
444 between wind and SLA.

445 We found that the influence of compound extreme conditions on SLA will amplify
446 in the future due to climate change. We showed that the intensity and frequency of
447 compound extreme conditions are projected to increase in the future under both
448 emission scenarios, especially at high latitudes where both precipitation and wind
449 intensity and frequency are expected to increase (Gastineau and Soden, 2009; Kao and
450 Ganguly, 2011). This results in higher SLA during these conditions compared to
451 historical ones when using historical thresholds. However, when using future thresholds
452 based on future distributions of precipitation and wind, we showed that SLA during
453 future compound extreme conditions is similar to historical ones. This indicates an
454 increase in the threshold for compound extreme conditions in the future relative to
455 historical ones.

456 It is important to acknowledge several limitations of our study that future research
457 could address. Firstly, one of the major shortcomings is the use of monthly mean data
458 instead of daily data. Monthly means may obscure the temporal dynamics and
459 intensities of compound extreme events, as they average out daily fluctuations. The
460 analysis of daily data would provide a more detailed understanding of the temporal
461 evolution and intensity of these conditions, as well as their specific impacts on sea level
462 anomalies. However, daily data are more volatile and contain more short-term noise,
463 and therefore may be more disturbing when used directly for long-term trend analysis.
464 Our study of long-term changes in the status of CWPEs tends to, and monthly data
465 provide more reliable and representative long-term trend information. Secondly, while
466 we examined the intensity and frequency of precipitation and wind extremes, we did
467 not specifically consider wind direction in our analysis. Wind direction is a crucial
468 factor that influences coastal flooding, as it determines the direction and intensity of
469 storm surges and waves. The inclusion of wind direction in future studies would provide
470 a more comprehensive picture of the combined effects of precipitation, wind speed, and



471 wind direction on sea level anomalies and coastal flooding risks. Addressing these
472 limitations through future research would help refine our understanding of compound
473 extreme conditions and their impacts on coastal regions.

474 Our findings have important implications for assessing the risks and impacts of
475 compound extreme conditions on coastal areas. Coastal areas are susceptible to
476 flooding due to sea level rise, storm surges, waves, tides, or river runoff (Becker et al.,
477 2023; Bevacqua et al., 2019). Compound extreme conditions can aggravate these risks
478 by increasing SLA during these conditions. Our results imply that coastal areas may
479 experience more frequent and intense compound extreme conditions in the future due
480 to climate change, which may increase their exposure and vulnerability to coastal
481 flooding. Therefore, it is crucial to consider compound extreme conditions in evaluating
482 coastal hazards, adaptation strategies, resilience planning. In summary, these findings
483 have important implications for understanding the impacts of compound extreme
484 conditions on a global scale and for assessing and managing the risks of coastal flooding
485 due to compound extreme conditions.

486

487 **Data Availability**

488 The CMIP6 climate data layer for the 11 GCMs were obtained from the WCRP Coupled
489 Model Intercomparison Project (Phase 6) (<https://esgf-node.llnl.gov/search/cmip6/>).
490 ECMFW ERA5 data were obtained from Copernicus Climate Data Store
491 ([https://cds.climate.copernicus.eu/cdsapp#!/dataset/reanalysis-era5-single-levels-
492 monthly-means?tab=overview](https://cds.climate.copernicus.eu/cdsapp#!/dataset/reanalysis-era5-single-levels-monthly-means?tab=overview)). Sea level gridded data from satellite observations were
493 obtained from the Copernicus Climate Change Service
494 ([https://cds.climate.copernicus.eu/cdsapp#!/dataset/satellite-sea-level-
495 global?tab=overview](https://cds.climate.copernicus.eu/cdsapp#!/dataset/satellite-sea-level-global?tab=overview)). Coastline data were obtained from Natural Earth
496 ([https://www.naturalearthdata.com/downloads/110m-physical-vectors/110m-
497 coastline/](https://www.naturalearthdata.com/downloads/110m-physical-vectors/110m-coastline/)).

498

499 **Authors' contributions**

500 Xinlong Zhang: Conceptualization, Formal analysis, Investigation, Methodology,
501 Writing – original draft. Jiayi Fang: Conceptualization, Methodology, Writing – review
502 & editing. Yue Qin: Conceptualization, Methodology, Writing – review & editing.
503 Weiping Wang: Conceptualization, Formal analysis, Investigation, Methodology,



504 Writing – review & editing. Ping Shen: Conceptualization, Formal analysis,
505 Investigation, Methodology, Writing – review & editing, Funding acquisition.

506

507 **Competing interests**

508 The authors declare that they have no known competing financial interests or personal
509 relationships that could have appeared to influence the work reported in this paper.

510

511 **Acknowledgement**

512 The authors greatly acknowledge the financial support from National Natural Science
513 Foundation of China (72001018 and 42001096), the Science Technology Department
514 of Zhejiang Province (No. 2022C03107), and Science and Technology Development
515 Fund, Macao SAR (Grant no. 001/2024/SKL). This work was also performed in part at
516 SICCC which is supported by SKL-IOTSC, University of Macau.

517

518 **Reference**

- 519 Back, L. E. and Bretherton, C. S.: The Relationship between Wind Speed and
520 Precipitation in the Pacific ITCZ, *J Clim*, 18, 4317–4328,
521 <https://doi.org/10.1175/JCLI3519.1>, 2005.
- 522 Becker, M., Karpytchev, M., and Hu, A.: Increased exposure of coastal cities to sea-
523 level rise due to internal climate variability, *Nature Climate Change* 2023 13:4, 13, 367–
524 374, <https://doi.org/10.1038/s41558-023-01603-w>, 2023.
- 525 Bermúdez, M., Farfán, J. F., Willems, P., and Cea, L.: Assessing the Effects of Climate
526 Change on Compound Flooding in Coastal River Areas, *Water Resour Res*, 57,
527 e2020WR029321, <https://doi.org/10.1029/2020WR029321>, 2021.
- 528 Bevacqua, E., Maraun, D., Vousdoukas, M. I., Voukouvalas, E., Vrac, M., Mentaschi,
529 L., and Widmann, M.: Higher probability of compound flooding from precipitation and
530 storm surge in Europe under anthropogenic climate change, *Sci Adv*, 5,
531 https://doi.org/10.1126/SCIADV.AAW5531/SUPPL_FILE/AAW5531_SM.PDF, 2019.
- 532 Bevacqua, E., Vousdoukas, M. I., Zappa, G., Hodges, K., Shepherd, T. G., Maraun, D.,
533 Mentaschi, L., and Feyen, L.: More meteorological events that drive compound coastal
534 flooding are projected under climate change, *Communications Earth & Environment*
535 2020 1:1, 1, 1–11, <https://doi.org/10.1038/s43247-020-00044-z>, 2020.
- 536 Bevacqua, E., De Michele, C., Manning, C., Couasnon, A., Ribeiro, A. F. S., Ramos, A.
537 M., Vignotto, E., Bastos, A., Blesić, S., Durante, F., Hillier, J., Oliveira, S. C., Pinto, J.



- 538 G., Ragno, E., Rivoire, P., Saunders, K., van der Wiel, K., Wu, W., Zhang, T., and
539 Zscheischler, J.: Guidelines for Studying Diverse Types of Compound Weather and
540 Climate Events, *Earths Future*, 9, e2021EF002340,
541 <https://doi.org/10.1029/2021EF002340>, 2021.
- 542 Bui, H. X., Li, Y.-X., Maloney, E. D., Kim, J.-E., Lee, S.-S., and Yu, J.-Y.: Emergence
543 of Madden-Julian oscillation precipitation and wind amplitude changes in a warming
544 climate, *npj Climate and Atmospheric Science* 2023 6:1, 6, 1–6,
545 <https://doi.org/10.1038/s41612-023-00344-z>, 2023.
- 546 Chen, F. and Zhang, Y.: On the coupling strength between the land surface and the
547 atmosphere: From viewpoint of surface exchange coefficients, *Geophys Res Lett*, 36,
548 <https://doi.org/10.1029/2009GL037980>, 2009.
- 549 Chen, L. S., Li, Y., and Cheng, Z. Q.: An overview of research and forecasting on
550 rainfall associated with landfalling tropical cyclones, *Adv Atmos Sci*, 27, 967–976,
551 <https://doi.org/10.1007/S00376-010-8171-Y/METRICS>, 2010.
- 552 Chen, X., Hossain, F., and Leung, L. R.: Probable Maximum Precipitation in the U.S.
553 Pacific Northwest in a Changing Climate, *Water Resour Res*, 53, 9600–9622,
554 <https://doi.org/10.1002/2017WR021094>, 2017.
- 555 Davison, B. J., Hogg, A. E., Rigby, R., Veldhuijsen, S., van Wessem, J. M., van den
556 Broeke, M. R., Holland, P. R., Selley, H. L., and Dutrieux, P.: Sea level rise from West
557 Antarctic mass loss significantly modified by large snowfall anomalies, *Nature*
558 *Communications* 2023 14:1, 14, 1–13, <https://doi.org/10.1038/s41467-023-36990-3>,
559 2023.
- 560 Deb, M., Sun, N., Yang, Z., Wang, T., Judi, D., Xiao, Z., and Wigmosta, M. S.:
561 Interacting Effects of Watershed and Coastal Processes on the Evolution of Compound
562 Flooding During Hurricane Irene, *Earths Future*, 11, e2022EF002947,
563 <https://doi.org/10.1029/2022EF002947>, 2023.
- 564 Dykstra, S. L. and Dzwonkowski, B.: The Role of Intensifying Precipitation on Coastal
565 River Flooding and Compound River-Storm Surge Events, Northeast Gulf of Mexico,
566 *Water Resour Res*, 57, e2020WR029363, <https://doi.org/10.1029/2020WR029363>,
567 2021.
- 568 Gabarró, C., Hughes, N., Wilkinson, J., Bertino, L., Bracher, A., Diehl, T., Dierking, W.,
569 Gonzalez-Gambau, V., Lavergne, T., Madurell, T., Malnes, E., and Wagner, P. M.:
570 Improving satellite-based monitoring of the polar regions: Identification of research and
571 capacity gaps, *Frontiers in Remote Sensing*, 4, 952091,
572 <https://doi.org/10.3389/FRSEN.2023.952091/BIBTEX>, 2023.
- 573 Gastineau, G. and Soden, B. J.: Model projected changes of extreme wind events in
574 response to global warming, *Geophys Res Lett*, 36,
575 <https://doi.org/10.1029/2009GL037500>, 2009.



- 576 Gori, A., Lin, N., Xi, D., and Emanuel, K.: Tropical cyclone climatology change greatly
577 exacerbates US extreme rainfall–surge hazard, *Nature Climate Change* 2022 12:2, 12,
578 171–178, <https://doi.org/10.1038/s41558-021-01272-7>, 2022.
- 579 Hersbach, H., Bell, B., Berrisford, P., Hirahara, S., Horányi, A., Muñoz-Sabater, J.,
580 Nicolas, J., Peubey, C., Radu, R., Schepers, D., Simmons, A., Soci, C., Abdalla, S.,
581 Abellan, X., Balsamo, G., Bechtold, P., Biavati, G., Bidlot, J., Bonavita, M., De Chiara,
582 G., Dahlgren, P., Dee, D., Diamantakis, M., Dragani, R., Flemming, J., Forbes, R.,
583 Fuentes, M., Geer, A., Haimberger, L., Healy, S., Hogan, R. J., Hólm, E., Janisková, M.,
584 Keeley, S., Laloyaux, P., Lopez, P., Lupu, C., Radnoti, G., de Rosnay, P., Rozum, I.,
585 Vamborg, F., Villaume, S., and Thépaut, J. N.: The ERA5 global reanalysis, *Quarterly*
586 *Journal of the Royal Meteorological Society*, 146, 1999–2049,
587 <https://doi.org/10.1002/QJ.3803>, 2020.
- 588 Hoegh-Guldberg, O., Jacob, D., Taylor, M., Guillén Bolaños, T., Bindi, M., Brown, S.,
589 Camilloni, I. A., Diedhiou, A., Djalante, R., Ebi, K., Engelbrecht, F., Guiot, J., Hijikata,
590 Y., Mehrotra, S., Hope, C. W., Payne, A. J., Pörtner, H. O., Seneviratne, S. I., Thomas,
591 A., Warren, R., and Zhou, G.: The human imperative of stabilizing global climate
592 change at 1.5°C, *Science* (1979), 365,
593 https://doi.org/10.1126/SCIENCE.AAW6974/SUPPL_FILE/AAW6974_HOEGH-
594 [GULDBERG_SM.PDF](https://doi.org/10.1126/SCIENCE.AAW6974/SUPPL_FILE/AAW6974_HOEGH-GULDBERG_SM.PDF), 2019.
- 595 Jiang, J., Zhou, T., Chen, X., and Zhang, L.: Future changes in precipitation over
596 Central Asia based on CMIP6 projections, *Environmental Research Letters*, 15, 054009,
597 <https://doi.org/10.1088/1748-9326/AB7D03>, 2020.
- 598 Kao, S. C. and Ganguly, A. R.: Intensity, duration, and frequency of precipitation
599 extremes under 21st-century warming scenarios, *Journal of Geophysical Research:*
600 *Atmospheres*, 116, 16119, <https://doi.org/10.1029/2010JD015529>, 2011.
- 601 Knutson, T. R., McBride, J. L., Chan, J., Emanuel, K., Holland, G., Landsea, C., Held,
602 I., Kossin, J. P., Srivastava, A. K., and Sugi, M.: Tropical cyclones and climate change,
603 *Nature Geoscience* 2010 3:3, 3, 157–163, <https://doi.org/10.1038/ngeo779>, 2010.
- 604 Lionello, P., Conte, D., and Reale, M.: The effect of cyclones crossing the
605 Mediterranean region on sea level anomalies on the Mediterranean Sea coast, *Natural*
606 *Hazards and Earth System Sciences*, 19, 1541–1564, <https://doi.org/10.5194/NHESS->
607 [19-1541-2019](https://doi.org/10.5194/NHESS-19-1541-2019), 2019.
- 608 Maduwantha, P., Wahl, T., Santamaria-Aguilar, S., Jane, R., Booth, J. F., Kim, H., and
609 Villarini, G.: A multivariate statistical framework for mixed storm types in compound
610 flood analysis, *Natural Hazards and Earth System Sciences*, 24, 4091–4107,
611 <https://doi.org/10.5194/NHESS-24-4091-2024>, 2024.
- 612 Martín, A., Amores, A., Orfila, A., Toomey, T., and Marcos, M.: Coastal extreme sea
613 levels in the Caribbean Sea induced by tropical cyclones, *Natural Hazards and Earth*



- 614 System Sciences, 23, 587–600, <https://doi.org/10.5194/NHESS-23-587-2023>, 2023.
- 615 Martius, O., Pfahl, S., and Chevalier, C.: A global quantification of compound
616 precipitation and wind extremes, *Geophys Res Lett*, 43, 7709–7717,
617 <https://doi.org/10.1002/2016GL070017>, 2016.
- 618 Messmer, M. and Simmonds, I.: Global analysis of cyclone-induced compound
619 precipitation and wind extreme events, *Weather Clim Extrem*, 32, 100324,
620 <https://doi.org/10.1016/J.WACE.2021.100324>, 2021.
- 621 Meucci, A., Young, I. R., Hemer, M., Kirezci, E., and Ranasinghe, R.: Projected 21st
622 century changes in extreme wind-wave events, *Sci Adv*, 6, 7295–7305,
623 https://doi.org/10.1126/SCIADV.AAZ7295/SUPPL_FILE/AAZ7295_SM.PDF, 2020.
- 624 Mora, C., Spirandelli, D., Franklin, E. C., Lynham, J., Kantar, M. B., Miles, W., Smith,
625 C. Z., Freel, K., Moy, J., Louis, L. V., Barba, E. W., Bettinger, K., Frazier, A. G.,
626 Colburn IX, J. F., Hanasaki, N., Hawkins, E., Hirabayashi, Y., Knorr, W., Little, C. M.,
627 Emanuel, K., Sheffield, J., Patz, J. A., and Hunter, C. L.: Broad threat to humanity from
628 cumulative climate hazards intensified by greenhouse gas emissions, *Nature Climate
629 Change* 2018 8:12, 8, 1062–1071, <https://doi.org/10.1038/s41558-018-0315-6>, 2018.
- 630 Moustakis, Y., Papalexiou, S. M., Onof, C. J., and Paschalis, A.: Seasonality, Intensity,
631 and Duration of Rainfall Extremes Change in a Warmer Climate, *Earths Future*, 9,
632 e2020EF001824, <https://doi.org/10.1029/2020EF001824>, 2021.
- 633 Muis, S., Verlaan, M., Winsemius, H. C., Aerts, J. C. J. H., and Ward, P. J.: A global
634 reanalysis of storm surges and extreme sea levels, *Nature Communications* 2016 7:1, 7,
635 1–12, <https://doi.org/10.1038/ncomms11969>, 2016.
- 636 Ridder, N. N., Pitman, A. J., Westra, S., Ukkola, A., Hong, X. Do, Bador, M., Hirsch,
637 A. L., Evans, J. P., Di Luca, A., and Zscheischler, J.: Global hotspots for the occurrence
638 of compound events, *Nature Communications* 2020 11:1, 11, 1–10,
639 <https://doi.org/10.1038/s41467-020-19639-3>, 2020.
- 640 Shaw, T. A., Baldwin, M., Barnes, E. A., Caballero, R., Garfinkel, C. I., Hwang, Y. T.,
641 Li, C., O’Gorman, P. A., Rivière, G., Simpson, I. R., and Voigt, A.: Storm track
642 processes and the opposing influences of climate change, *Nature Geoscience* 2016 9:9,
643 9, 656–664, <https://doi.org/10.1038/ngeo2783>, 2016.
- 644 Vousdoukas, M. I., Clarke, J., Ranasinghe, R., Reimann, L., Khalaf, N., Duong, T. M.,
645 Ouweneel, B., Sabour, S., Iles, C. E., Trisos, C. H., Feyen, L., Mentaschi, L., and
646 Simpson, N. P.: African heritage sites threatened as sea-level rise accelerates, *Nature
647 Climate Change* 2022 12:3, 12, 256–262, <https://doi.org/10.1038/s41558-022-01280-1>,
648 2022.
- 649 Wahl, T., Jain, S., Bender, J., Meyers, S. D., and Luther, M. E.: Increasing risk of
650 compound flooding from storm surge and rainfall for major US cities, *Nature Climate
651 Change* 2015 5:12, 5, 1093–1097, <https://doi.org/10.1038/nclimate2736>, 2015.



- 652 Waliser, D. and Guan, B.: Extreme winds and precipitation during landfall of
653 atmospheric rivers, *Nature Geoscience* 2017 10:3, 10, 179–183,
654 <https://doi.org/10.1038/ngeo2894>, 2017.
- 655 Walsh, J. E., Ballinger, T. J., Euskirchen, E. S., Hanna, E., Mård, J., Overland, J. E.,
656 Tangen, H., and Vihma, T.: Extreme weather and climate events in northern areas: A
657 review, *Earth Sci Rev*, 209, 103324,
658 <https://doi.org/10.1016/J.EARSCIREV.2020.103324>, 2020.
- 659 Woodworth, P. L., Melet, A., Marcos, M., Ray, R. D., Wöppelmann, G., Sasaki, Y. N.,
660 Cirano, M., Hibbert, A., Huthnance, J. M., Monserrat, S., and Merrifield, M. A.: Forcing
661 Factors Affecting Sea Level Changes at the Coast, *Surveys in Geophysics* 2019 40:6,
662 40, 1351–1397, <https://doi.org/10.1007/S10712-019-09531-1>, 2019.
- 663 Wu, J., Shi, Y., and Xu, Y.: Evaluation and Projection of Surface Wind Speed Over
664 China Based on CMIP6 GCMs, *Journal of Geophysical Research: Atmospheres*, 125,
665 e2020JD033611, <https://doi.org/10.1029/2020JD033611>, 2020.
- 666 Yaddanapudi, R., Mishra, A., Huang, W., and Chowdhary, H.: Compound Wind and
667 Precipitation Extremes in Global Coastal Regions Under Climate Change, *Geophys Res*
668 *Lett*, 49, e2022GL098974, <https://doi.org/10.1029/2022GL098974>, 2022.
- 669 Zha, J., Wu, J., Zhao, D., and Fan, W.: Future projections of the near-surface wind speed
670 over eastern China based on CMIP5 datasets, *Clim Dyn*, 54, 2361–2385,
671 <https://doi.org/10.1007/S00382-020-05118-4/TABLES/4>, 2020.
- 672 Zittis, G., Almazroui, M., Alpert, P., Ciais, P., Cramer, W., Dahdal, Y., Fnais, M., Francis,
673 D., Hadjinicolaou, P., Howari, F., Jrrar, A., Kaskaoutis, D. G., Kulmala, M., Lazoglou,
674 G., Mihalopoulos, N., Lin, X., Rudich, Y., Sciare, J., Stenchikov, G., Xoplaki, E., and
675 Lelieveld, J.: Climate Change and Weather Extremes in the Eastern Mediterranean and
676 Middle East, *Reviews of Geophysics*, 60, e2021RG000762,
677 <https://doi.org/10.1029/2021RG000762>, 2022.
- 678 Zscheischler, J. and Seneviratne, S. I.: Dependence of drivers affects risks associated
679 with compound events, *Sci Adv*, 3,
680 https://doi.org/10.1126/SCIADV.1700263/SUPPL_FILE/1700263_SM.PDF, 2017.
- 681 Zscheischler, J., Martius, O., Westra, S., Bevacqua, E., Raymond, C., Horton, R. M.,
682 van den Hurk, B., AghaKouchak, A., Jézéquel, A., Mahecha, M. D., Maraun, D., Ramos,
683 A. M., Ridder, N. N., Thiery, W., and Vignotto, E.: A typology of compound weather
684 and climate events, *Nature Reviews Earth & Environment* 2020 1:7, 1, 333–347,
685 <https://doi.org/10.1038/s43017-020-0060-z>, 2020.
- 686 Zscheischler, J., Naveau, P., Martius, O., Engelke, S., and C. Raible, C.: Evaluating the
687 dependence structure of compound precipitation and wind speed extremes, *Earth*
688 *System Dynamics*, 12, 1–16, <https://doi.org/10.5194/ESD-12-1-2021>, 2021.
- 689 Zubier, K. M. and Eyouni, L. S.: Investigating the Role of Atmospheric Variables on

<https://doi.org/10.5194/egusphere-2024-3799>

Preprint. Discussion started: 20 January 2025

© Author(s) 2025. CC BY 4.0 License.



690 Sea Level Variations in the Eastern Central Red Sea Using an Artificial Neural Network

691 Approach, Oceanologia, 62, 267–290,

692 <https://doi.org/10.1016/J.OCEANO.2020.02.002>, 2020.

693